ISSN 0020-1685, Inorganic Materials, 2016, Vol. 52, No. 2, pp. 153–162. © Pleiades Publishing, Ltd., 2016.
Original Russian Text © T.A. Sedneva, M.L. Belikov, E.P. Lokshin, A.T. Belyaevskii, 2016, published in Neorganicheskie Materialy, 2016, Vol. 52, No. 2, pp. 187–196.

Synthesis and Physicochemical Properties of Titanium(IV)- and Cobalt(II)-Based Photocatalytic Oxide Composites

T. A. Sedneva, M. L. Belikov, E. P. Lokshin, and A. T. Belyaevskii

Tananaev Institute of Chemistry and Technology of Rare Elements and Minerals, Kola Scientific Center, Russian Academy of Sciences, Akademgorodok 26a, Apatity, Murmansk oblast, 184209 Russia

e-mail: sedneva@chemy.kolasc.net.ru

Received March 26, 2015; in final form, June 17, 2015

Abstract—We have studied the phase transitions, morphology, and photocatalytic activity of composites based on titanium(IV) and cobalt(II) oxides at Co doping levels from 0.5 to 60 wt % and heat-treatment temperatures from 80 to 1150°C. The highest photocatalytic activity under illumination in the spectral range $\lambda \geq 670$ nm is offered by mesoporous X-ray amorphous and multiphase (X-ray amorphous phase, anatase, rutile, and $CoTiO_3$) nanomaterials containing 5–20 wt % Co, whereas two-phase materials (rutile + $CoTiO_3$) have the lowest photocatalytic activity.

DOI: 10.1134/S0020168516010143

INTRODUCTION

The need for more efficient solar power conversion in photocatalytic processes of organic contamination destruction by TiO_2, a well-known photocatalyst, requires improving its photocatalytic activity (PCA) in the visible range by creating titania-based oxide composites with a band gap under 3.1 eV, characteristic of undoped TiO_2. In connection with this, the development of techniques for modifying the optical properties of TiO_2 in the spectral range $\lambda > 400$ nm is of practical interest [1, 2].

The extension of the spectral range of PCA to the visible and infrared spectral regions by doping TiO_2 with the aliovalent ions W^{6+} and Nb^{5+} was the subject of previous studies [3, 4]. It is reasonable to expect that titania-based nanocomposites containing cobalt oxide (band gap of 0.7 eV [5]) will be active in the visible range.

Cobalt catalysts promoted with various metal oxides, such as Co/Al_2O_3, Co/MgO, Co/ThO, Co/K_2O, and Co/TiO_2 [6], are widely used in the preparation of chemical products: gasoline, oil, paraffin, ethylene, potable alcohol, and others.

The synthesis and application of photocatalytic CoO/TiO_2 oxide composites have been the subject of relatively few reports. In particular, Zhang Guoge et al. [7] demonstrated enhanced PCA of a CoO/TiO_2 nanotube composite produced by cathode deposition of titania in 0.05 M $Co(NO_3)_2$ onto carbon nanotubes annealed at 450°C. Enhanced PCA of Co-doped titania powders prepared by a sol–gel process was also reported by Xu Rui et al. [8]. TiO_2/Co photocatalyst films annealed at 400°C were reported to have enhanced PCA for methylene blue degradation [9]. Co migration into TiO_2 in the films was ensured by physical vaporization during heat treatment of alternating TiO_2 and Co layers. Surkin et al. [10] described a technique for the preparation of glasses having multilayer titanium-containing coatings with improved functional and performance characteristics, using high-temperature (500–700°C) heat treatment, which produced a dense, crystalline TiO_2 film containing impurity ions, including Co, penetrating the titania layer via diffusion from intermediate layers. Yu-Fen Wang et al. [11] discussed nonaqueous synthesis of CoO_x/TiO_2 dispersions with high photocatalytic performance.

Known methods for the fabrication of such structures using mechanical doping or sol–gel processing have insufficient technological feasibility for a number of reasons [8–11]. We expect alkaline cohydrolysis of Ti and Co salts to be a simpler and more efficient approach.

The purpose of this work was to investigate the key features of the formation of composites in the Ti–O–Co system at doping levels from 0.5 to 60 wt % Co with the aim of developing more readily available photocatalysts active in the visible spectral region.

EXPERIMENTAL

The composite materials for this investigation were prepared through the cohydrolysis of the $TiCl_4$ and $CoCl_2$ salts in aqueous ammonia at a temperature of 20 ± 2°C, using procedures described previously [3, 4]. The dopant concentration in the hydrolysis products was varied from 0.5 to 60 wt % Co. Heat treatment in air at temperatures from 80 to 1150°C yielded multiphase nanocomposites, which were characterized by chemical analysis, X-ray diffraction

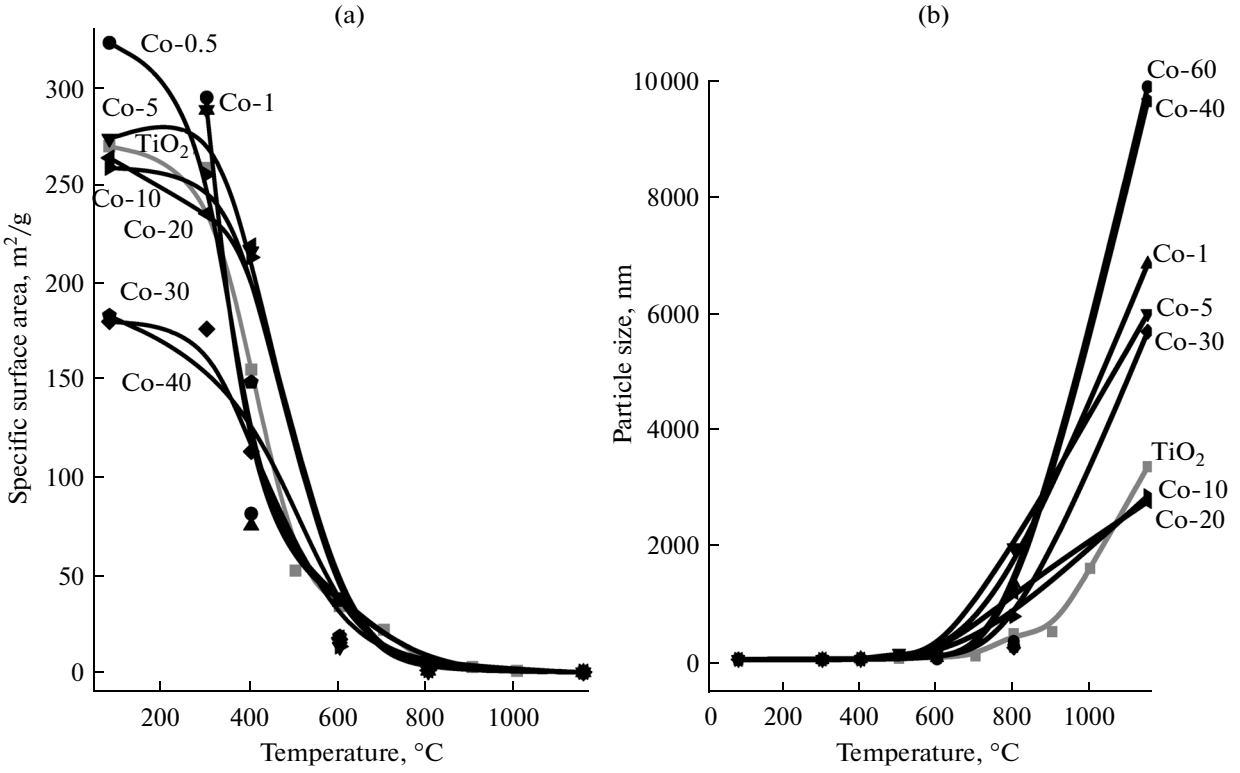

Fig. 1. (a) Specific surface area and (b) particle size as functions of heat-treatment temperature and Co content for Co-modified titanium dioxide samples.

(XRD) (DRON-3 diffractometer, CuK_α radiation), low-temperature nitrogen BET measurements (FlowSorb II 2300 and TriStar 3020 V1.03), thermogravimetry (TG) (Netzsch STA 409 PC/PG), and scanning electron microscopy (SEM) (SEM LEO-420). Their PCA was assessed photocolorimetrically (FEK-56 PM) from the degree of decoloration (E, %) of ferroin in response to illumination in the visible range and with $\lambda > 670$ nm light. The samples were identified by a code, for example, 400-Co-0.5, which specified the heat-treatment temperature (400°C), dopant (Co), and doping level (0.5 wt %).

RESULTS AND DISCUSSION

The experimental data presented in Tables 1–4 and Figs. 1–7 illustrate the influence of heat-treatment conditions (t, °C) and Co content (wt %) on the chemical composition, phase composition (XRD data), specific surface area (S, m^2/g), average particle size (d, nm), pore volume (V, cm^3/g), pore depth (h, nm), and pore diameter (D, nm) of our samples and their PCA (E, %) for an indicator degradation reaction under illumination in the visible range and with $\lambda \geq 670$ 670 nm light.

Doping of TiO_2 with 0.5–60 wt % Co ensures the preparation of nanopowders (7–12 nm) with a specific surface area from 180 to 320 m^2/g, containing up to 6.6 wt % NH_4^+ and 1.06 wt % Cl^-. At low doping levels (0.5–1.0 wt % Co), the hydrolysis products contain about 79.9 wt % TiO_2, which is closely consistent with the formula of the titanium oxyhydroxide $TiO(OH)_2$ (81.6 wt % TiO_2). Raising the heat treatment temperature leads to a systematic decrease in NH_4^+ and Cl^- content, an increase in particle size, and, as a consequence, a reduction in the specific surface area of the powders (Table 1, Fig. 1).

Phase formation. XRD data (Table 1, Fig. 2) indicated that the hydrolysis products were X-ray amorphous. The differential scanning calorimetry (DSC) curves of the Co-modified materials (Fig. 3) were similar to that of TiO_2 [11], indicating, in combination with chemical analysis data, that the salt cohydrolysis products had an oxyhydroxide nature.

Independent of the Co doping level, all of the DSC curves had a single endothermic peak, corresponding to dehydration of the hydrolysis products. Chemical analysis data indicated simultaneous removal of volatile components: chloride ions and ammonium group (Table 1). The dehydration was mostly complete at temperatures around the exothermic peak, with a weight loss in the samples from ≈22 to ≈28% (Table 2), which included the loss of the volatile components.

As suggested by XRD data (Fig. 2), the strong exothermic peak in the DSC curves can be interpreted as

Table 1. Phase composition and physicochemical properties of composites in the Ti–O–Co system

Sample	t, °C	Weight percent				XRD results	S, m^2/g	d, nm
		TiO_2	Cl^-	NH_4^+	Co^{2+}		BET	
80-Co-0.5	80	79.1	–	–	0.26	am	323	7.1
400-Co-0.5	400	–	–	–	–	a	82	19
700-Co-0.5	700	–	–	–	–	20% a., 80% r	–	–
800-Co-0.5	800	–	–	–	–	r	1.05	1360
1150-Co-0.5	1150	–	–	–	–	r	0.24	5950
80-Co-1	80	78.6	–	–	0.43	am	–	–
300-Co-1	300	–	–	–	–	am	288	8.0
400-Co-1	400	–	–	–	–	a	75	20
600-Co-1	600	98.8			0.97	99% a, 1% r	36	39
700-Co-1	700	–	–	–	–	10% a, 90% r	–	–
1150-Co-1	1150	–	–	–	–	r	0.21	6800
80-Co-5	80	79.8	–	3.28	1.67	am	274	8.4
400-Co-5	400	–	–	0.34	–	a, am	216	7.1
500-Co-5	500	–	–	–	–	95% a, 5% r	14	114
600-Co-5	600	94.7	–	–	4.9	a, r, $CoTiO_3$	13.4	111
800-Co-5	800	–	–	–	–	r, $CoTiO_3$	0.74	1930
1150-Co-5	1150	–	–	–	–	r, $CoTiO_3$	0.24	5950
80-Co-10	80	71.9	ND	4.51	5.14	am	264	8.7
400-Co-10	400	–	–	0.46	–	am	219	10
600-Co-10	600	88.8	ND	ND	9.84	a, r, $CoTiO_3$	18	55
700-Co-10	700	–	–	–	–	r, $CoTiO_3$	–	–
800-Co-10	800	–	–	–	–	r, $CoTiO_3$	1.17	1160
1150-Co-10	1150	–	–	–	–	r, $CoTiO_3$	0.35	2720
80-Co-20	80	–	–	–	–	am	259	8.9
400-Co-20	400	–	–	–	–	am	213	11
600-Co-20	600	80.2	–	–	19.8	a, r, $CoTiO_3$	13	74
800-Co-20	800	–	–	–	–	r, $CoTiO_3$	1.33	747
1150-Co-20	1150	–	–	–	–	r, $CoTiO_3$	0.34	2820
80-Co-30	80	64.7	–	–	–	am	180	13
400-Co-30	400	–	0.3	0.15	–	am	113	20
600-Co-30	600	83.9	ND	ND		a, r, $CoTiO_3$	17	58
800-Co-30	800	–	–	–	–	r, $CoTiO_3$	4.54	211
1150-Co-30	1150					r, $CoTiO_3$	0.17	5640
80-Co-40	80	64.6	–	6.60	–	am	183	13
400-Co-40	400	–	–	0.20	–	am	149	16
500-Co-40	500	–	–	–	–	a, r, $CoTiO_3$	35	28
600-Co-40	600	76.8	–	–	–	a, r, $CoTiO_3$	19	53
800-Co-40	800	–	–	–	–	r, $CoTiO_3$	4.21	228
1150-Co-40	1150	–	–	–	–	r, $CoTiO_3$	0.12	9600
80-Co-60	80	–	–	–	–	–	254	9.1
400-Co-60	400	–	–	–	–	am	156	15
600-Co-60	600	41.9	–	–	45.7	a, r, $CoTiO_3$	21	73
800-Co-60	800	–	–	–	–	r, $CoTiO_3$	4.45	321
1110-Co-60	1150	–	–	–	–	r, $CoTiO_3$	0.11	9850

am = amorphous as determined by X-ray diffraction, a = anatase, r = rutile, ND = not detected; the symbol – denotes that no determination was made.

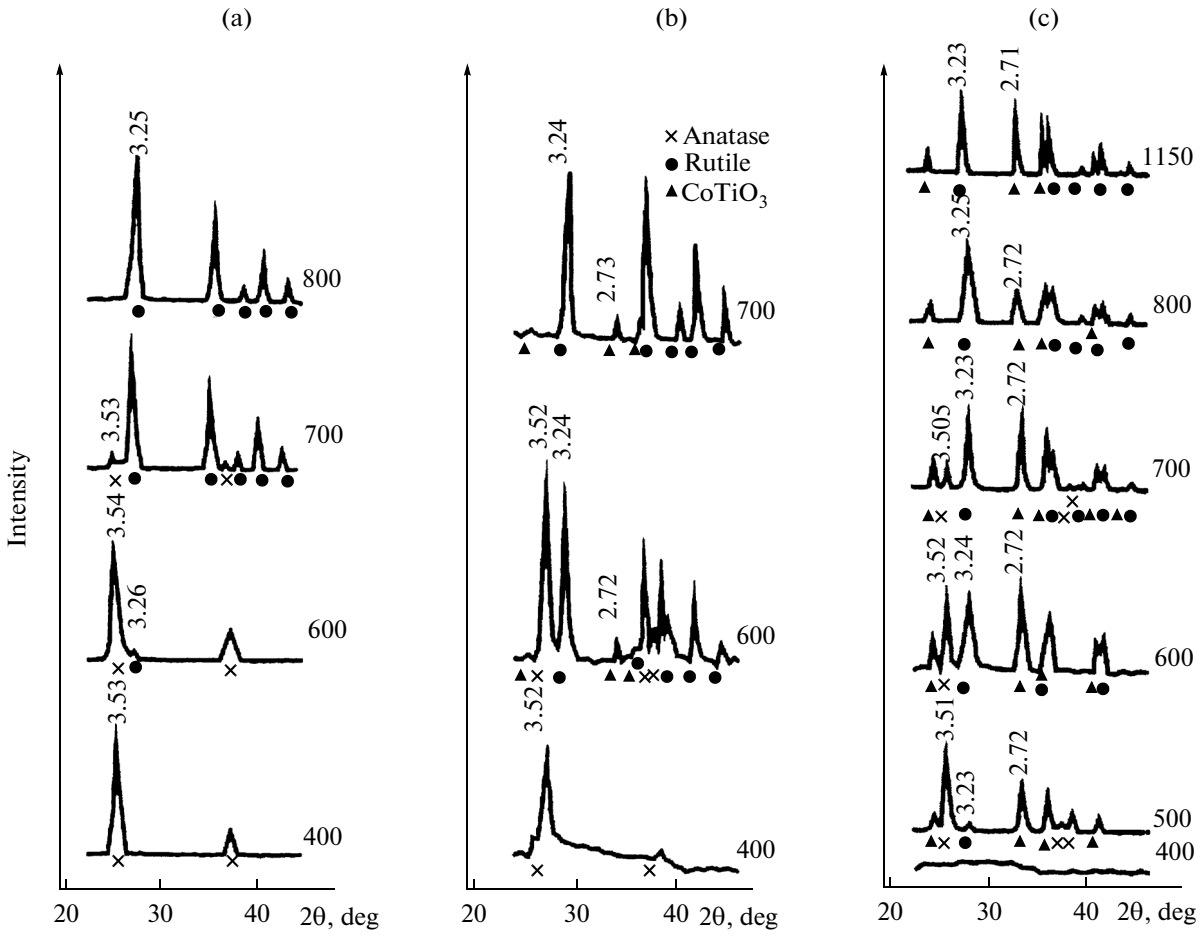

Fig. 2. X-ray diffraction patterns of Co-modified titanium dioxide at various heat-treatment temperatures (numbers at the scans, degrees Celsius) and Co doping levels: (a) 1, (b) 5, and (c) 40 wt % Co.

evidence of simultaneous crystallization processes: the formation of cobalt-containing anatase and transformation of the anatase into rutile, accompanied by cobalt release in the form of the $CoTiO_3$ metatitanate (Fig. 3, Table 2). The increase in the temperature of the exothermic peak due to crystallization from 424.3 to 527.3°C as the cobalt content increases from 0.5 to 40 wt % may be due to specific features of Co: the crystallization of cobalt oxides requires high energy consumption [12]. The same is evidenced by the diffraction patterns in Fig. 2: as the Co doping level increases from 1 to 40 wt %, reflections from anatase, a crystalline phase, disappear in the XRD patterns of the samples calcined at 400°C (Fig. 2c).

As the temperature is raised from 400 to 1150°C, XRD data demonstrate a number of phase transitions of TiO_2, which depend on the Co doping level. At doping levels of 1 wt % Co or lower, XRD data indicate only the formation of anatase (3.52 Å) and then rutile (3.24 Å) at a temperature of ≃700°C. A small amount of $CoTiO_3$ that is presumably formed together with the above phases cannot be detected by X-ray diffraction. At Co doping levels above 5 wt % and temperatures near the exothermic peak, we observe the anatase–rutile phase transition, accompanied by cobalt precipitation in the form of $CoTiO_3$ (2.72 Å). It is reasonable to assume that Co has a promoting effect on the rutile formation process. In particular, an increase in doping level from 0.5 to 10 wt % Co is accompanied by a decrease in the temperature of the anatase–rutile phase transition from 700 to 500°C and cobalt metatitanate crystallization. Note that, over the entire range of doping levels examined, no cobalt oxides were detected, and the cobalt crystallized only as $CoTiO_3$.

Thus, a characteristic feature of the synthesis products in the Ti–O–Co system is the formation of several phases, depending on the doping level and heat-treatment temperature (Fig. 4).

Morphology. The specific surface area of the hydrolysis products was 180–330 m^2/g (particle size, 7–13 nm); that of the anatase + rutile + cobalt metatitanate mixed-phase materials was smaller, 36–70 m^2/g (40–57 nm), and that of the rutile + cobalt metatitanate two-phase composites did not exceed 0.1–4.5 m^2/g (0.3–10 μm). Thus, at heat-treatment temperatures below 800–900°C, both the X-ray amor-

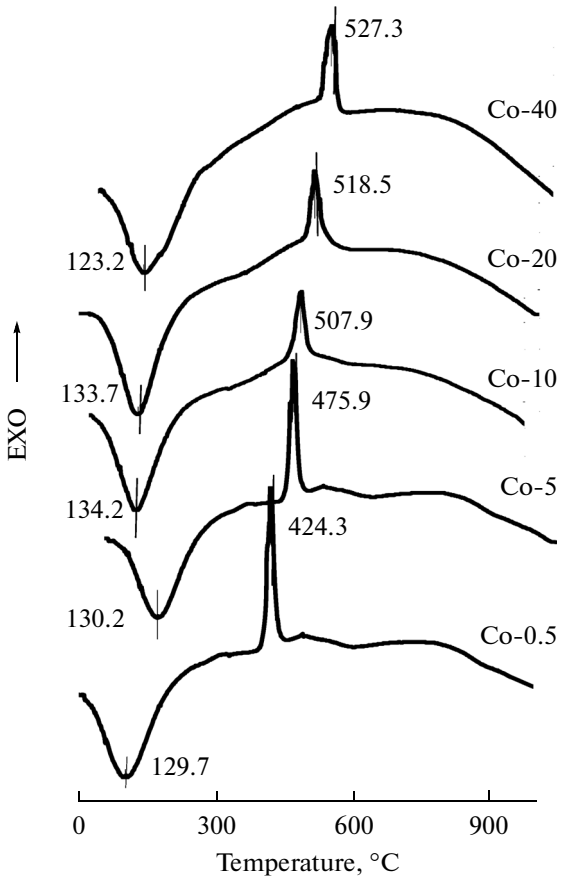

Fig. 3. DSC curves of Co-modified TiO_2 samples at various Co doping levels.

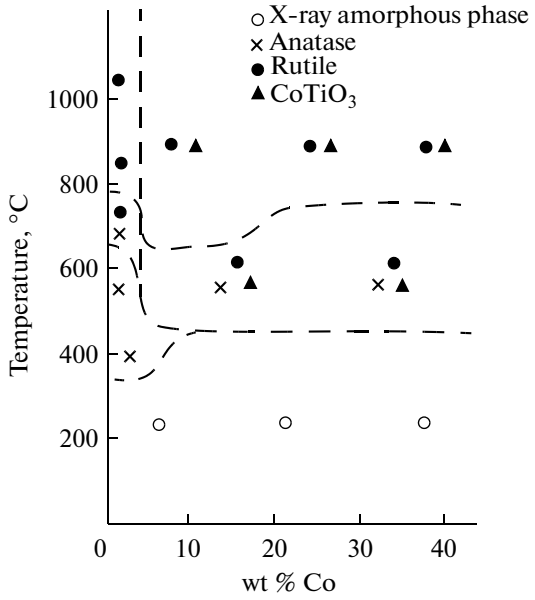

Fig. 4. Phase composition of the synthesized composites in relation to Co content and heat-treatment temperature.

phous powders and multiphase composites had a large surface area and nanoscale character. With the development of the agglomeration process at temperatures above 900°C, the particle size of the powders increased to microns (Table 1).

The texture characteristics of some of the synthesized composites are summarized in Table 3 and Fig. 5. The samples with incomplete dehydration were similar in texture characteristics. The pore depth and diameter in the samples heat-treated at 400°C or lower temperatures were comparable: for example, 4.47 and 4.30 nm, respectively, in the 400-Co-20 sample.

In the range 80–800°C, the micropore volume V as a function of temperature has extrema, which is possibly the consequence of the rapid water removal from the oxyhydroxide hydrolysis products. Next, the pore volume decreases because of the agglomeration. The micropore volume in the X-ray amorphous materials

Table 2. Thermal events and XRD data in the Ti–O–Co system

Sample	DSC		Δm, % (TG at t_{max})	XRD	
	t_{min}, °C	t_{max}, °C		d_{hkl}, Å, at t_{max}	phase
Co-0.5	129.7	427.3	22.2	**3.52,** 2.38	Anatase
Co-5	130.2	475.9	28.5	**3.52**, 2.38	Anatase
				3.71, **2.73**, 2.53	$CoTiO_3$
Co-10	134.2	507.9	27.5	**3.52**, 2.38	Anatase
				3.25, 2.50	Rutile
				3.71, **2.73**, 2.53	$CoTiO_3$
Co-20	133.7	518.5	24.6	**3.52**, 2.38	Anatase
				3.25, 2.50	Rutile
				3.71, **2.73**, 2.53	$CoTiO_3$
Co-40	123.2	527.3	23.5	**3.52**, 2.38	Anatase
				3.25, 2.50	Rutile
				3.71, **2.73**, 2.53	$CoTiO_3$

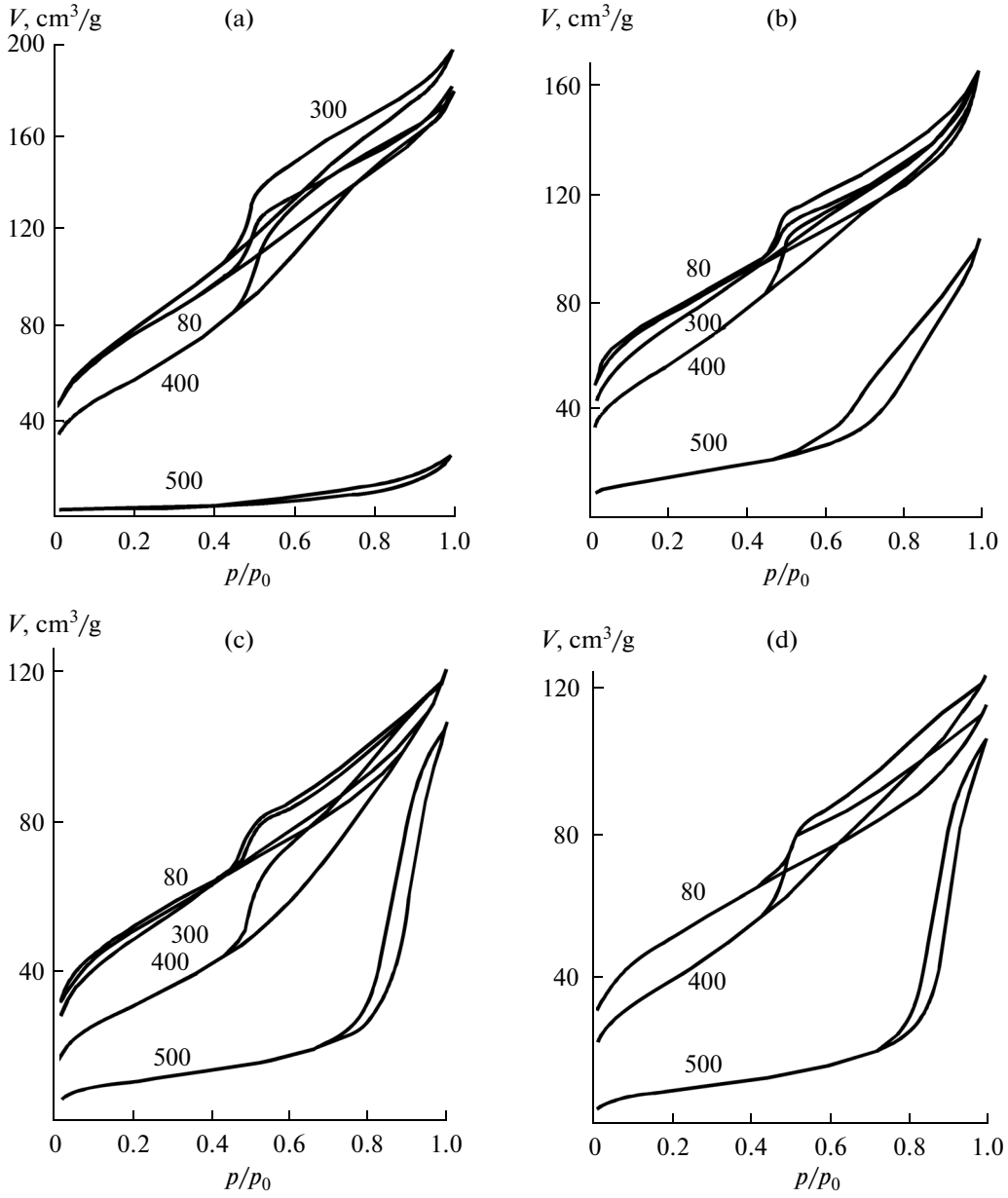

Fig. 5. Sorption isotherms of the synthesized composites after heat treatment at various temperatures (specified at the curves in degrees Celsius) in relation to Co content: (a) 5, (b) 20, (c) 30, and (d) 40 wt % Co.

ranges from 0.15 to 0.29 cm^3/g. As the temperature is raised to above 600°C, the pore diameter increases more rapidly than the pore depth: 7.9 and 20.4 nm in the 800-Co-20 sample. In particular, the micropore volume in the 800-Co-60 sample is as small as 0.024 cm^3/g. At the same time, it is worth noting that increasing the Co content of the samples helps to maintain the micropore size at elevated temperatures as well.

The sorption isotherms of both the X-ray amorphous and crystalline samples (Fig. 5) have the form of S-shaped absorption–desorption curves with hysteresis loops, which point to a mesoporous nature of the composites [13]. The onset of crystallization processes reduces the mesoporosity of the powders. The sorption curves of the composites calcined at temperatures above 900°C have negligible hysteresis.

Thus, both the X-ray amorphous and crystalline multiphase composites in the Ti–O–Co system with a specific surface area from about 15 to 330 m^2/g have a mesoporous structure. Mesoporous materials are thought to have considerable potential as catalysts for conversion of three-dimensional organic molecules, because the presence of mesopores may help to overcome diffusion limitations [13] characteristic of micropores.

Table 3. Influence of cobalt content and heat-treatment temperature on the texture characteristics (V, h, and D) of Co-modified TiO_2 samples

t,°C	V, cm^3/g	h, nm	D, nm	t,°C	V, cm^3/g	h, nm	D, nm
Co-0.5				Co-1			
80	–	–	–	80	0.29	3.71	3.97
300	0.27	3.39	4.09	300	0.29	4.09	3.84
400	0.19	9.03	6.95	400	0.18	8.85	6.86
600	–	–	–	500	0.054	9.15	7.05
Co-5				Co-10			
80	0.26	3.93	4.12	80	0.22	3.60	4.11
300	0.29	4.11	3.99	300	0.22	3.79	3.96
400	0.28	4.96	4.32	400	0.26	4.60	4.20
500	0.042	10.4	8.82	500	0.049	11.4	9.76
Co-20				Co-30			
80	0.22	3.66	4.40	80	0.16	3.95	4.43
300	0.23	3.80	4.11	300	0.17	3.99	4.26
400	0.25	4.47	4.30	400	0.19	6.24	5.06
500	0.16	10.5	8.68	500	0.16	16.9	13.6
Co-40				Co-60			
80	0.15	3.75	4.18	80	0.158	2.98	3.40
400	0.19	4.94	4.33	300	–	–	–
500	0.16	17.5	13.8	400	0.173	4.49	3.78
600	–	–	–	600	0.158	28.41	24.75
800	0.019	7.9	20.4	800	0.024	8.30	20.96

SEM images of the Co-containing materials obtained at heat-treatment temperatures in the range from 400 to 1150°C (Fig. 6) demonstrate that the materials have broad particle size distributions. The X-ray amorphous materials consist of irregularly shaped, large, layered aggregates of nanoparticles. With increasing heat-treatment temperature, the particle size increases in all of the samples, and the particles form separate rounded crystallites. At 1150°C, they sinter to form large agglomerates (up to tens of microns in size) having bumps with smooth surfaces, indicative of mesopore collapse because of the rapid growth and agglomeration of indistinguishable rutile and $CoTiO_3$ crystals.

Photocatalytic activity. According to our preliminary results, the PCA of the Co-modified titanium dioxide samples for ferroin degradation in suspensions exposed to visible light is a rather strong and intricate function of the doping level, heat-treatment temperature, and phase composition. Almost all of the Co-modified TiO_2 samples exhibit higher PCA than does the commercially available photocatalyst AEROXIDE P25, manufactured by Degussa (P25), under illumination with the entire solar spectrum and, especially, with filtered light in the range $\lambda \geq 670$ nm, which nominally corresponds to a reduction in the band gap of the composites to 1.85 eV (Table 4, Fig. 7).

Note that the highest PCA is offered by the mesoporous X-ray amorphous and multiphase samples with the largest specific surface area, whereas the two-phase samples consisting of only rutile and cobalt metatitanate, which have the smallest specific surface area, with no mesoporosity, exhibit the lowest PCA. Clearly, the spectral sensitization of the nanocomposites to longer wavelengths is due the Co in combination with the phase states of TiO_2.

The composition dependences of PCA for the composites obtained at 600°C or lower temperatures

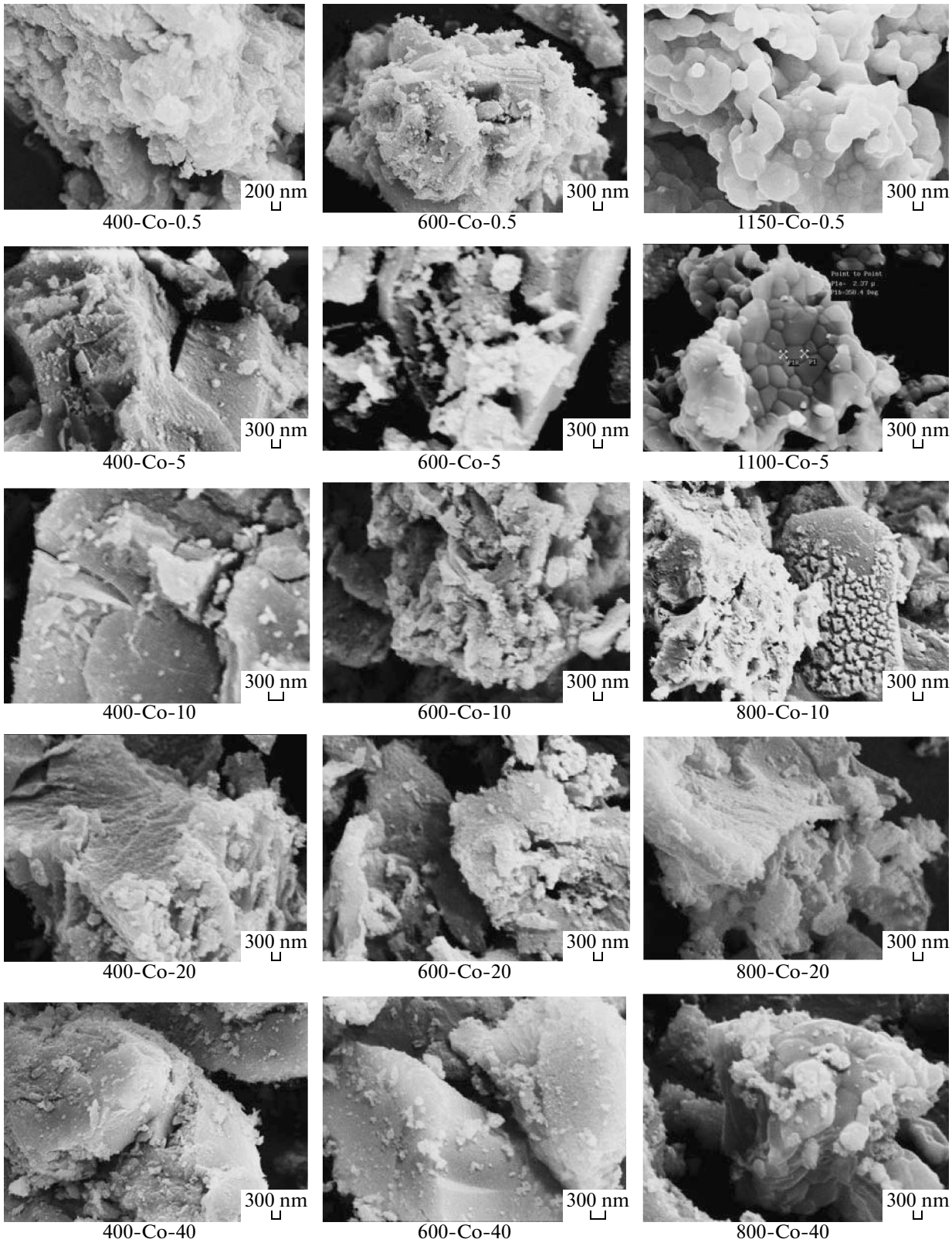

Fig. 6. SEM micrographs of the surface of composite particles synthesized at temperatures from 400 to 1150°C (see Fig. 4 for the phase compositions of the particles).

Table 4. Influence of Co content, heat-treatment temperature, phase composition, and particle size on the PCA (*E*, %) of Co-modified TiO_2 samples for ferroin under illumination in the visible range and with $\lambda \geq 670$ nm light

Sample	XRD	*d*, nm	*E*, %	
			visible light	$\lambda \geq 670$ nm
P25	86% a, 14% r	30	45	0
400-TiO_2	a	9.9	94	47
80-Co-1	am	–	96	78
400-Co-1	a	20	82	61
600-Co-1	99% a, 1% r	39	77	59
800-Co-1	r	1320	60	47
1150-Co-1	r	6800	58	46
80-Co-5	am	8.4	96	91
400-Co-5	am, a	7.1	89	82
600-Co-5	a, r, $CoTiO_3$	13	76	70
800-Co-5	r, $CoTiO_3$	0.74	56	52
1150-Co-5	r, $CoTiO_3$	0.24	54	49
80-Co-10	am	8.7	100	96
400-Co-10	am	10	92	89
600-Co-10	a, r, $CoTiO_3$	55	81	77
800-Co-10	r, $CoTiO_3$	1160	68	65
1150-Co-10	r, $CoTiO_3$	2720	62	58
80-Co-20	am	8.9	95	90
400-Co-20	am	11	87	84
600-Co-20	a, r, $CoTiO_3$	74	82	77
800-Co-20	r, $CoTiO_3$	747	69	65
1150-Co-20	r, $CoTiO_3$	2820	62	54
80-Co-40	am	13	77	67
400-Co-40	am	20	74	66
600-Co-40	a, r, $CoTiO_3$	58	77	67
800-Co-40	r, $CoTiO_3$	211	76	65
1150-Co-40	r, $CoTiO_3$	5640	62	56
80-Co-60	am	9.1	69	57
400-Co-60	am	15	66	54
600-Co-60	a, r, $CoTiO_3$	73	58	51
800-Co-60	r, $CoTiO_3$	321	54	47
1150-Co-60	r, $CoTiO_3$	9850	55	44

a = anatase, r = rutile, am = amorphous as determined by X-ray diffraction.

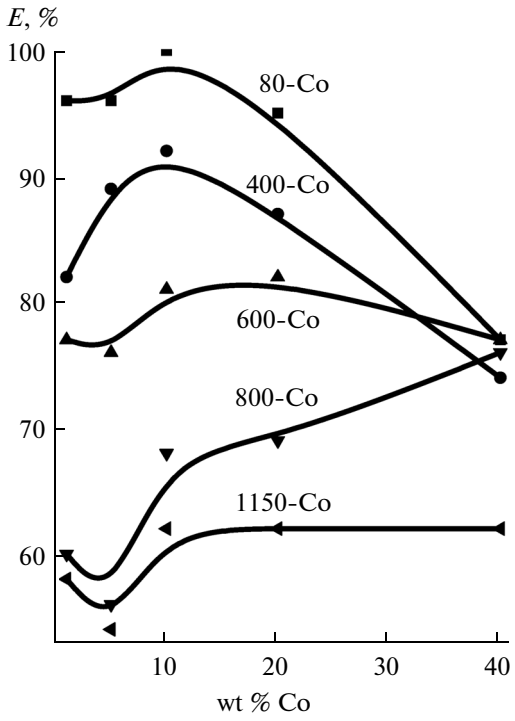

Fig. 7. PCA isotherms of the synthesized composites at various Co doping levels.

(Fig. 7) have extrema. Doping in the range 10–20 wt % Co was found to increase the PCA of the composites. The rather high PCA of the samples calcined at temperatures near 600°C suggests the possibility of regenerating photocatalysts through the thermolysis of organic compounds.

CONCLUSIONS

We have studied the phase transitions, morphology, and PCA of composites based on titanium(IV) and cobalt(II) oxides at Co doping levels from 0.5 to 60 wt % and heat-treatment temperatures from 80 to 1150°C.

The highest PCA under illumination in the spectral range $\lambda \geq 670$ nm is offered by mesoporous X-ray amorphous and multiphase nanomaterials containing 5–20 wt % Co, whereas rutile and two-phase samples (rutile + cobalt metatitanate) have the lowest PCA. The nanocomposites may be X-ray amorphous or consist of various multiphase mixtures of X-ray amorphous phases, anatase, rutile, and cobalt metatitanate with a crystallite size of up to 100 nm.

Thus, the observed increase in PCA and spectral sensitization under illumination with light in the range $\lambda \geq 670$ nm are due to the formation of multiphase structures and to the fact that the addition of cobalt enhances the semiconducting properties of titanium dioxide.

ACKNOWLEDGMENTS

This work was supported by the RF Ministry of Education and Science (grant no. NSh 487.2014.3).

REFERENCES

1. Fenezonov, V.B. and Parmon, V.N., Introduction to the physical chemistry of texturing of heterogeneous photocatalysts, in *Promyshlennyi kataliz v lektsiyakh* (Lectures on Industrial Catalysis), Moscow: Kalvis, 2005, part 1.
2. Jin, Q., Fujishima, M., and Tada, H., Visible-light-active iron oxide-modified anatase titanium(IV) dioxide, *J. Phys. Chem. C*, 2011, vol. 115, no. 14, pp. 6478–6483.
3. Sedneva, T.A., Lokshin, E.P., Kalinnikov, V.T., and Belikov, M.L., Photocatalytic activity of tungsten-modified titanium oxide, *Dokl. Phys. Chem.*, 2012, vol. 443, no. 1, pp. 57–59.
4. Sedneva, T.A., Lokshin, E.P., Belikov, M.L., and Belyaevskii, A.T., TiO_2- and Nb_2O_5-based photocatalytic composites, *Inorg. Mater.*, 2013, vol. 49, no. 4, pp. 382–389.
5. Samsonov, G.V., Bulankova, T.G., and Burykina, A.L., *Fiziko-khimicheskie svoistva okislov. Spravochnik* (Physicochemical Properties of Oxides: A Handbook), Moscow: Metallurgiya, 1969.
6. Lapidus, A.L., Krylova, A.Yu., Kozlova, G.V., and Kondrat'ev, L.T., Effect of oxide additives on the activity of cobalt carbonyl catalysts for the synthesis of hydrocarbons from CO and H_2, *Izv. Akad. Nauk SSSR, Neorg. Mater.*, 1989, vol. 25, no. 11, pp. 2425–2428.
7. Zhang Guoge, Huang Haitao, Li Wenfang, Yu Fei, Wu Huijun, and Zhou Limin, Enhanced photocatalytic activity of CoO/TiO_2 nanotube composite, *Electrochim. Acta*, 2012, vol. 81, pp. 117–122.
8. Xu Rui, Li Jia, Wang Jun, Wang Xiaofang, Liu Bin, Wang Baoxin, Luan Xiaoyu, and Zhang Xiangdong, Photocatalytic degradation of Er^{3+} organic dyes under solar light irradiation combined with Er^{3+}:$YAlO_3$/Fe- and Co-doped TiO_2 coated composites, *Sol. Energy Mater. Sol. Cells*, 2010, vol. 94, no. 6, pp. 1157–1165.
9. Carvalho Hudson, W.P., Batista Ana, P.L., Bertholdo, R., Santilli Celso, V., Pulcinelli Sandra, H., and Ramalho Teodorico, C., Photocatalyst TiO_2–Co: the effect of doping depth profile on methylene blue degradation, *J. Mater. Sci.*, 2010, vol. 45, no. 20, pp. 5698–5703.
10. Surkin, R.R., Zhimalov, A.B., Bondareva, L.N., Gorina, I.N., Gerancheva, O.E., and Polkan, G.A., RF Patent 2434819, *Byull. Izobret.*, 2011, no. 33.
11. Yu-Fen Wang, Meng-Chun Hsieh, Jyh-Fu Lee, and Chia-Min Yan, Nonaqueous synthesis of CoO_x/TiO_2 nanocomposites showing high photocatalytic activity of hydrogen generation, *Appl. Catal., B*, 2013, vols. 142–143, pp. 626–632.
12. Ivanova, V.P., Kasatov, B.K., Krasavina, T.N., and Rozinova, E.L., *Termicheskii analiz mineralov i gornykh porod* (Thermal Analysis of Minerals and Rocks), Leningrad: Nedra, 1974.
13. Gregg, S.J. and Sing, K.S.W., *Adsorption, Surface Area, and Porosity*, New York: Academic, 1982.

Translated by O. Tsarev